VIP Photocatalysis

DOI: 10.1002/anie.201301306

$Cu_2(OH)PO_4$, a Near-Infrared-Activated Photocatalyst**

Gang Wang, Baibiao Huang, Xiangchao Ma, Zeyan Wang, Xiaoyan Qin, Xiaoyang Zhang, Ying Dai, and Myung-Hwan Whangbo*

Under ultraviolet (UV) light, TiO_2 is a superb photocatalyst that is resistant to photochemical or chemical corrosion.[1–3] However, it is ineffective under sunlight because the latter has less than ca. 5% UV light. Sunlight consists of about 48% visible light, so there have been numerous efforts to develop photocatalysts that are effective under visible light, which include N-doped TiO_2 photocatalysts,[4,5] plasmonic photocatalysts,[6–8] and dye-sensitized photocatalysts for water-splitting.[9–11] Compared with efforts to utilize the visible region of sunlight, studies aimed at utilizing near-infrared (NIR) light, despite the fact that NIR constitutes about 44% of sunlight, are rather rare. Qin et al.[12] reported the photocatalytic activity of YF_3:Yb,Tm/TiO_2 under NIR light; YF_3 particles doped with Yb and Tm absorb NIR light and emit a weak UV light, which then excites TiO_2 to promote photocatalysis. This up-conversion photocatalyst has very low photocatalytic efficiency and is difficult to prepare. To the best of our knowledge, there is no known NIR-driven photocatalyst that does not require the up-conversion of NIR light energy.

In this work we show that libethenite, $Cu_2(OH)PO_4$, strongly absorbs energy in the NIR region and is an effective photocatalyst for the oxidation of 2,4-dichlorophenol (2,4-DCP) in aqueous solution under NIR light irradiation ($\lambda > 800$ nm). This is accomplished through study of the electronic structure of $Cu_2(OH)PO_4$, in which axially elongated $CuO_4(OH)_2$ octahedra share their corners with axially compressed $CuO_4(OH)$ trigonal bipyramids, as depicted in Figure 1.

Figure 2a shows typical scanning electron microscopy (SEM) images of the $Cu_2(OH)PO_4$ microcrystals. The lath-shaped crystals are about 4–5 μm in length and 1.5 μm in width, with ravines on the surface that are long, narrow, and shallow. The XRD pattern in Figure 2b shows that the sample is highly crystalline. All of the diffraction peaks can be indexed to the orthorhombic phase of $Cu_2(OH)PO_4$ (JCPDS No. 360404)[13] with the lattice constants $a = 8.43$ Å, $b = 8.08$ Å, and $c = 5.90$ Å.

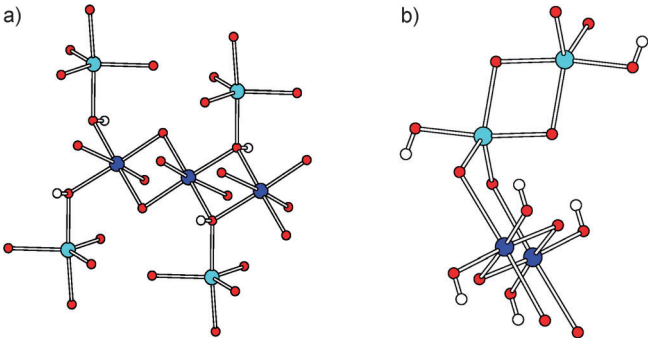

Figure 1. Views showing the corner-sharing between $CuO_4(OH)_2$ octahedra and $CuO_4(OH)$ trigonal bipyramids in $Cu_2(OH)PO_4$. For $CuO_4(OH)_2$ octahedra, O red, H white, and Cu blue; for $CuO_4(OH)$ trigonal bipyramids, Cu cyan. a) Corner-sharing through OH groups; b) Corner-sharing through O atoms. All O atoms, except for those in the OH groups, are corner-shared with PO_4 tetrahedra. In each $CuO_4(OH)_2$ octahedron, the equatorial Cu–O bond lengths are 1.977 Å (×2) and 1.963 Å (×2), and the axial Cu–O bond lengths are 2.385 Å (×2). In each $CuO_4(OH)$ trigonal bipyramid, the equatorial Cu–O bond lengths are 2.040 Å and 2.051 Å (×2), and the axial Cu–O bond lengths are 1.926 Å (×2).

The UV/Vis/NIR absorption spectrum of the $Cu_2(OH)PO_4$ sample derived from its diffuse reflectance spectrum, which reveals a high absorption in the NIR region, is shown in Figure 3. The NIR absorption of $Cu_2(OH)PO_4$ can be fitted with four Gaussian peaks centered at 670, 864, 1121, and 1349 nm (at 1.85, 1.44, 1.11 and 0.92 eV, respectively). The absorption observed beyond 2000 nm is attributable to the lattice and OH stretching modes.[14,15]

The photocatalytic decomposition of 2,4-DCP in aqueous solution (20 mg L^{-1}) over $Cu_2(OH)PO_4$ microcrystals was probed under NIR ($\lambda > 800$ nm) irradiation. The temperature of the solution was maintained at 20–25 °C to minimize the loss of 2,4-DCP by evaporation during extended NIR irradiation. Our results, summarized in Figure 3b and c, show that $Cu_2(OH)PO_4$ microcrystals effectively decompose 2,4-DCP in solution under NIR light irradiation, with 90% removal after 6 h irradiation time. The state of the Cu in the $Cu_2(OH)PO_4$ sample measured by XPS before and after the photocatalytic reactions was identical, as shown in Figure 3d; the Cu $2p_{3/2}$ had a main peak at about 935.0 eV before the reaction, and at 934.9 eV after it.

The photocatalytic reaction of $Cu_2(OH)PO_4$ requires an effective way of separating the electron–hole pair generated by NIR light absorption. To gain insight into this question, we examined the electronic band structure of $Cu_2(OH)PO_4$ by

[*] G. Wang, Prof. Dr. B. Huang, Z. Wang, X. Qin, Prof. X. Zhang
State Key Lab of Crystal Materials, Shandong University
Jinan 250100 (China)
E-mail: bbhuang@sdu.edu.cn
Homepage: http://www.icm.sdu.edu.cn/index.php
X. Ma, Prof. Dr. Y. Dai
School of physics, Shandong University (China)
Prof. Dr. M.-H. Whangbo
Department of Chemistry, North Carolina State University
Raleigh, NC 276955-8204 (USA)

[**] This work was financially supported by the National Basic Research Program of China (973 Program, No.2013CB632401) and the National Natural Science Foundation of China (Nos. 20973102, 51021062 and 51002091).

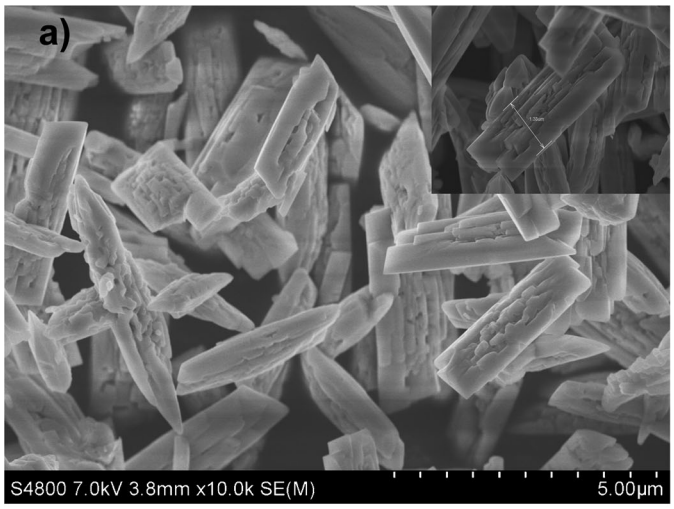

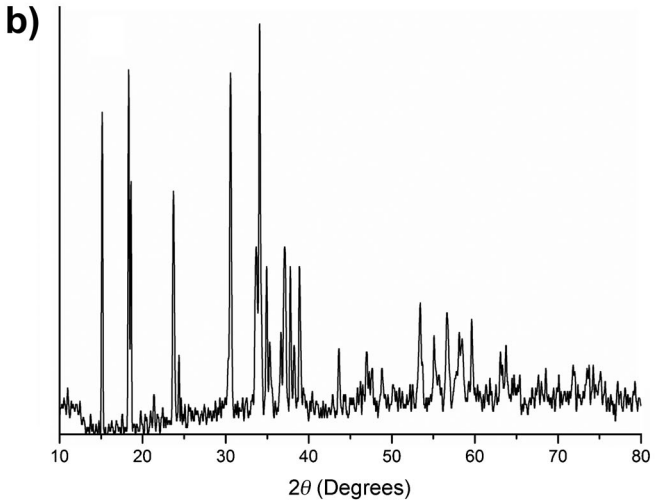

Figure 2. a) SEM image of $Cu_2(OH)PO_4$ microcrystals; b) XRD pattern of $Cu_2(OH)PO_4$.

performing density functional theory (DFT) calculations.[16,17] The resulting electronic structure should have a band gap, because $Cu_2(OH)PO_4$ is a magnetic insulator.[18] Thus, we carried out DFT plus on-site repulsion U (DFT + U) calculations[19] with effective on-site repulsion $U^{eff} = U - J = 3$, 4, and 5 eV. The optical excitation energies best matching the observed NIR absorption are obtained from the use of $U^{eff} =$ 3 eV, so our discussion below is based on these results. Figure 4 presents our results in plots of total density of states (TDOS) and projected density of states (PDOS). The Cu^{2+} (d^9) ion at each $CuO_4(OH)$ trigonal bipyramid and at each $CuO_4(OH)_2$ octahedron has one singly filled d level (the d_{z^2} at the trigonal bipyramid with the local z axis along the axial Cu–O bonds, and the $d_{x^2-y^2}$ at the octahedron with the local x and y axes along the equatorial Cu–O bonds). In the DFT + U calculations these levels lead to the four unoccupied down-spin bands that appear as four TDOS peaks in Figure 4. The optical excitations in these bands are possible only from the occupied down-spin bands. In the following, therefore, our discussion will be confined to the down-spin bands.

The highest occupied band has a strong contribution from the O 2p states (Figure 4a), and strong Cu 3d contributions occur at ca. 2.0 eV below the Fermi level (Figure 4a). Each peak of the four unoccupied bands has Cu 3d and O 2p contributions from the trigonal pyramids, as well as from the octahedra (Figure 4a,b), as does the highest-occupied band (Figure 4a,b). This feature is necessary for optical excitation to take place from the highest occupied band to the four unoccupied bands, which are responsible for the strong NIR light absorption. (in Figure 3a, the NIR absorption spectrum was fitted with four Gaussian peaks.) The electrons excited from the highest occupied to the upper parts of the four unoccupied bands will eventually cascade down to the lowest-lying unoccupied band. The highest-occupied band has much stronger Cu 3d and O 2p contributions from the trigonal bipyramids than from the octahedra (Figure 4b,c). In the lowest-lying unoccupied band, the octahedral and the trigonal bipyramidal sites have nearly equal Cu 3d and O 2p contributions, with slightly greater contributions from the octahedra (Figure 4b and c). This suggests that the photo-generated electrons from the $CuO_4(OH)$ trigonal bipyramids are transferred to the $CuO_4(OH)_2$ octahedra. These polyhedra share their OH corners (Figure 1a), on which both the d_{z^2} orbital of $CuO_4(OH)$ and the $d_{x^2-y^2}$ orbital of $CuO_4(OH)_2$ have a substantial O 2p contribution. In the four unoccupied bands, the O 2p contribution from the OH groups is weak in the lowest-lying one, but strong in the upper three (Fig-

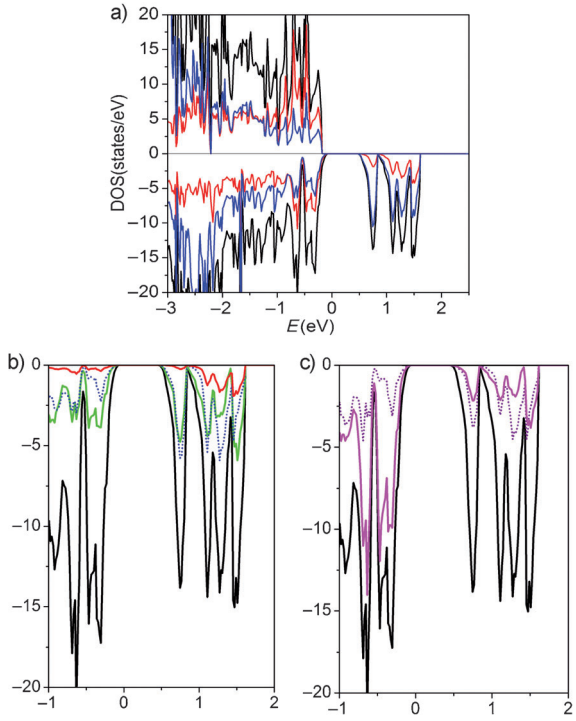

Figure 4. TDOS and PDOS plots calculated for $Cu_2(OH)PO_4$. a) The PDOS plots for the total Cu 3d (blue) and O 2p (red) states; TDOS (black). b) The PDOS plots for the O 2p states of the OH groups (red), the Cu 3d states of the octahedral Cu sites (blue dots), and those of the trigonal bipyramidal Cu sites (green); TDOS (black). c) The PDOS plots for the O 2p states of the O atoms belonging only to the $CuO_4(OH)_2$ octahedra (purple dots) and those belonging only to the $CuO_4(OH)$ trigonal bipyramids (pink); TDOS (black).

ure 4b). Thus, the photogenerated electrons from the $CuO_4(OH)$ trigonal bipyramids that reach the upper three unoccupied bands are easily transferred to the $CuO_4(OH)_2$ octahedra. Once they come down to the lowest-lying unoccupied band, they will be prevented from back-transferring to the adjacent trigonal bipyramidal sites, because the O 2p contribution from the OH groups is weak in that band (Figure 4b). Thus, the photogenerated electron-hole pairs in $Cu_2(OH)PO_4$ can be effectively separated and the photooxidation would take place in the vicinity of the $CuO_4(OH)$ trigonal bipyramids. For this to occur efficiently, the surface of $Cu_2(OH)PO_4$ exposed to the NIR irradiation should have both $CuO_4(OH)_2$ octahedra and $CuO_4(OH)$ square pyramids. This should be the case because, as the SEM image (Figure 2a) shows, there are plenty of ravines on the surface of the $Cu_2(OH)PO_4$ microcrystals. Thus, the mechanism for the photocatalytic reaction of $Cu_2(OH)PO_4$ under NIR irradiation can be summarized as follows, where TBP and OCT refer to trigonal bipyramidal and octahedral sites, respectively:

$$\text{TBP } Cu^{II} + h\nu \rightarrow \text{TBP } Cu^{III} + e^- \quad (1)$$

$$\text{OCT } Cu^{II} + e^- \rightarrow \text{OCT } Cu^{I} \quad (2)$$

$$\text{TBP } Cu^{III} + \text{2,4-DCP} \rightarrow \text{TBP } Cu^{II} + H_2O + CO_2 + H^+ + Cl^- \quad (3)$$

$$\text{OCT } Cu^{I} + H^+ + O_2 \rightarrow \text{OCT } Cu^{II} + H_2O \quad (4)$$

The electron–hole pairs generated at the $CuO_4(OH)$ trigonal bipyramids are separated by transferring the photogenerated electrons to the neighboring $CuO_4(OH)_2$ octahedra. Formally, this leads to Cu^{III} sites at the $CuO_4(OH)$ trigonal bipyramids and Cu^{I} sites at the $CuO_4(OH)_2$ octahedra. Then the Cu^{III} sites oxidize 2,4-DCP and, as a result, become Cu^{II}; whereas the Cu^{I} sites react with H^+ and O_2 in the solution, thus returning to Cu^{II} and completing the full photocatalytic circle.

In summary, $Cu_2(OH)PO_4$ strongly absorbs in the NIR region and is an effective photocatalyst that oxidizes 2,4-DCP in aqueous solution under NIR irradiation. The photocatalytic activity of $Cu_2(OH)PO_4$ is explained by an effective separation of the electron–hole pairs. Our work suggests that it would be promising to examine the transition-metal oxides with different coordination environments for the metal ions in the search for more NIR-activated photocatalysts.

Experimental Section

$Cu_2(OH)PO_4$ microcrystals were prepared by a hydrothermal method in which stoichiometric amounts of $Cu(NO_3)_2$ and Na_2HPO_4 were mixed into deionized water (ca. 80 mL) under constant stirring for 1 h, and then the pH of the suspension was adjusted to seven. The suspension was transferred into a 120 mL sealed teflon-lined autoclave and followed by hydrothermal treatment at 120 °C for 6 h. The sample was collected by filtration, then thoroughly washed with

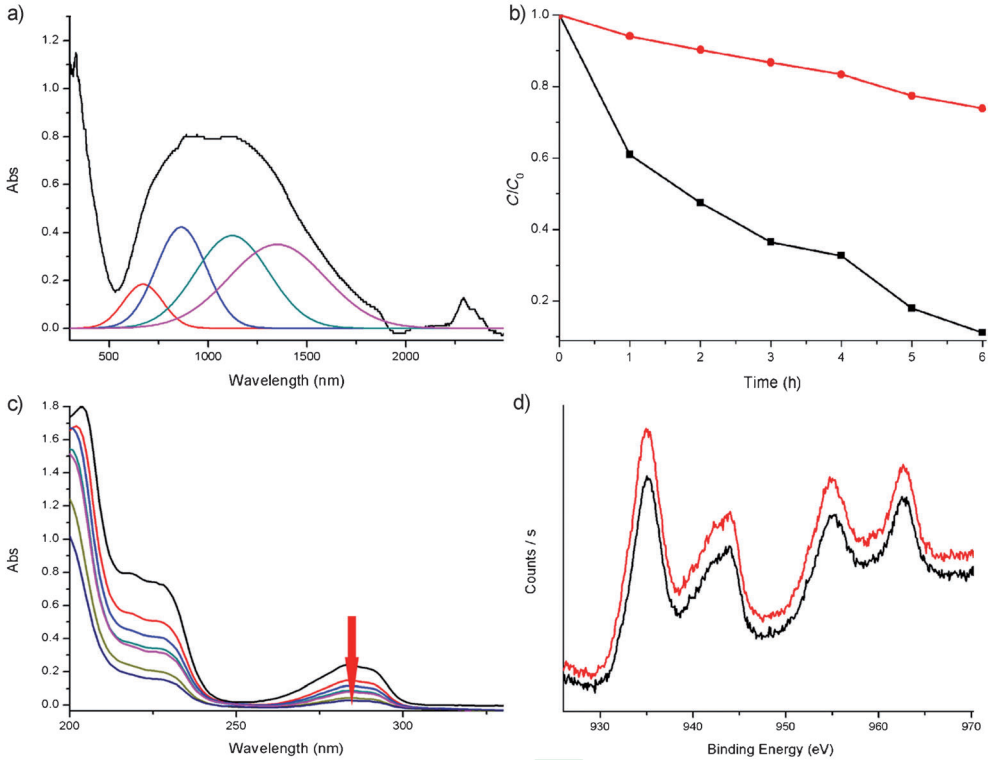

Figure 3. a) UV/Vis/NIR absorption spectrum of $Cu_2(OH)PO_4$, where the NIR region was fitted with four Gaussian peaks. Original (black), 670 nm (red), 864 nm (blue), 1121 nm (green), 1349 nm (pink). b) Photodegradation of 2,4-DCP in aqueous solution over $Cu_2(OH)PO_4$ microcrystals with NIR irradiation at 20–25 °C. The fraction of the concentration of 2,4-DCP that remains in the solution after irradiation is plotted as a function of the irradiation time. Loss of 2,4-DCP from photoctalytic decomposition (black squares), Loss of 2,4-DCP from volatilization (red circles). c) Absorption spectra of the aqueous solution of 2,4-DCP as a function of the irradiation time. 0 h (black), 1 h (red), 2 h (light blue), 3 h (green), 4 h (pink), 5 h (gold), 6 h (dark blue). The arrow (at ca. 284 nm) indicates the direction of increasing reaction time. d) XPS spectra of the Cu states of the $Cu_2(OH)PO_4$ sample before (black) and after (red) the photodegradation experiments.

deionized water and ethanol, and finally dried in an oven at 60 °C overnight.

Received: February 14, 2013
Published online: March 28, 2013

Keywords: copper · nanocrystals · near-infrared light · photocatalysts · photochemistry

[1] A. L. Linsebigler, G. Q. Lu, J. T. Yates, *Chem. Rev.* **1995**, *95*, 735 – 758.
[2] S. Kim, W. Choi, *J. Phys. Chem. B* **2005**, *109*, 5143 – 5149.
[3] G. K. Zhang, X. M. Ding, F. S. He, X. Y. Yu, J. Zhou, Y. J. Hu, J. W. Xie, *Langmuir* **2008**, *24*, 1026 – 1030.
[4] G. D. Yang, Z. Jiang, H. H. Shi, T. C. Xiao, Z. F. Yan, *J. Mater. Chem.* **2010**, *20*, 5301 – 5309.
[5] M. Mrowetz, W. Balcerski, A. J. Colussi, M. R. Hoffman, *J. Phys. Chem. B* **2004**, *108*, 17269 – 17273.
[6] P. Wang, B. B. Huang, X. Y. Qin, X. Y. Zhang, Ying. Dai, J. Y. Wei, M.-H. Whangbo, *Angew. Chem.* **2008**, *120*, 8049 – 8051; *Angew. Chem. Int. Ed.* **2008**, *47*, 7931 – 7933.
[7] Z. K. Zheng, B. B. Huang, X. Y. Qin, X. Y. Zhang, Y. Dai, J. Y. Wei, M.-H. Whangbo, *J. Mater. Chem.* **2011**, *21*, 9079 – 9087.
[8] For a recent review, see: P. Wang, B. B. Huang, Y. Dai, M. H. Whangbo, *Phys. Chem. Chem. Phys.* **2012**, *14*, 9813 – 9825.
[9] T. Kajiwara, K. Hashimoto, T. Kawai, T. Sakata, *J. Phys. Chem.* **1982**, *86*, 4516 – 4522.
[10] K. Hashimoto, T. Kawai, T. Sakata, *Chem. Lett.* **1983**, 709 – 712.
[11] T. Shimidzu, T. Iyoda, Y. Koide, *J. Am. Chem. Soc.* **1985**, *107*, 35 – 41.
[12] W. P. Qin, D. S. Zhang, D. Zhao, L. L. Wang, K. Z. Zheng, *Chem. Commun.* **2010**, *46*, 2304 – 2306.
[13] Y. Z. Zhan, H. L. Li, Y. L. Chen, *J. Hazard. Mater.* **2010**, *180*, 481 – 485.
[14] G. R. Hunt, J. W. Salisbury, *Mod. Geol.* **1970**, *1*, 283 – 300.
[15] G. R. Hunt, J. W. Salisbury, C. Lenhoff, *Mod. Geol.* **1971**, *2*, 195 – 205.
[16] Our spin-polarized DFT calculations employed the projector-augmented wave method coded in the Vienna ab initio simulation package,[17a–c] and the generalized gradient approximation of Perdew, Burke, and Ernzerhof[17d] for exchange and correlation corrections with plane wave cutoff energies of 400 eV, a set of $3\times3\times4$ k-points, and a threshold of self-consistent-field energy convergence of 10^{-4} eV.
[17] a) P. E. Blöchl, *Phys. Rev. B* **1994**, *50*, 17953 – 17979; b) G. Kresse, D. Joubert, *Phys. Rev. B* **1999**, *59*, 1758 – 1775; c) G. Kresse, J. Furthmüller, *Phys. Rev. B* **1996**, *54*, 11169 – 11186; d) J. P. Perdew, K. Burke, M. Ernzerhof, *Phys. Rev. Lett.* **1996**, *77*, 3865 – 3868.
[18] A. A. Belik, H. J. Koo, M. H. Whangbo, N. Tsujii, P. Naumov, E. Takayama-Muromachi, *Inorg. Chem.* **2007**, *46*, 8684.
[19] S. L. Dudarev, G. A. Botton, S. Y. Savrasov, C. J. Humphreys, A. P. Sutton, *Phys. Rev. B* **1998**, *57*, 1505 – 1509.

